Summer Student Report

10 October 2024
inkyu.hwang@cern.ch

TOF Spectrum Analysis of HCIs synthesized using antiprotons

Inkyu Hwang
Supervisors: Fredrik Parnefjord Gustafsson, Michael Doser
CERN, CH-1211, Geneva, Switzerland

Keywords: AEgIS, antiprotonic atom, highly charged radioactive ions, TOF spectrum

Summary

In the AEgIS experiment, we develop a technique for trapping radioactive HCIs (Highly Charged Ions) in a Penning-Malmberg trap, using antiprotons generated from the antiproton decelerator (AD) at CERN. By introducing slow antiprotons (<12keV) to gaseous molecules, the annihilation between the antiproton and the nucleus leads to nuclear fragmentation, which produces HCIs. These HCIs can be sensitive probes for QED, QCD, weak interaction, and nuclear structure. In this report, the TOF spectrum analysis aims to reveal the composition and distribution of synthesized ions.

Contents

1 Introduction

1.1 The AEgIS experiment

The AEgIS experiment (The Antimatter experiment - Gravity, Interferometry, Spectroscopy), located at the Antiproton Decelerator facility at CERN, focuses on the studies of antimatter-bound systems, such as the study of gravitational influence on antihydrogen, positronium, and recently, antiprotonic bound systems.

To understand the formation mechanism of antiprotonic atoms and resulting HCIs (highly charged ions), antiprotons were introduced into the AEgIS Penning-Malmberg trap filled with ultra-low density gas(10^{-8}mbar). The interaction between the antiprotons and gaseous molecules results in collisional ionization which decelerates the antiprotons to the point that antiprotons are now slow enough to be captured by the gas molecules, forming antiprotonic atoms. This process results in a rapid cascade of ejecting electrons, resulting in HCIs. This report includes the analysis result of the experiment where antiprotons were injected into Nitrogen and Argon gases.

1.2 Penning-Malmberg trap

In the AEgIS experiment, the Penning-Malmberg trap, known for its ability to confine a large number of single-charged particles, is used to trap antiprotons. Using this trap, we can also control electons and positrons on a regular basis.

A Penning-Malmberg trap consists of multiple cylindrical metal electrodes and magnets. At least three electrodes are required to trap a group of single charged ions. The strong axial magnetic field confines charged particles radially, and the longitudinal alignment of electrodes create electric field that traps particles axially. Throughout multiple scans, changes in the geometry (width) and potential (floor or wall potential) within the trap change the rate and timing of the formation of HCIs.

In the AEgIS experiment, several devices are installed on (or attached to) the trap to detect TOF and annihilation signals. In the Penning-Malmberg trap, electrodes are fed up to 10kV potential for axial confinement, with a magnetic field of 5T. Another trap, installed where the particle detector (MCP) is located, is maintained with a 1T magnetic field. Additional scintillation detectors surround the trap to measure pions that result from annihilation events.

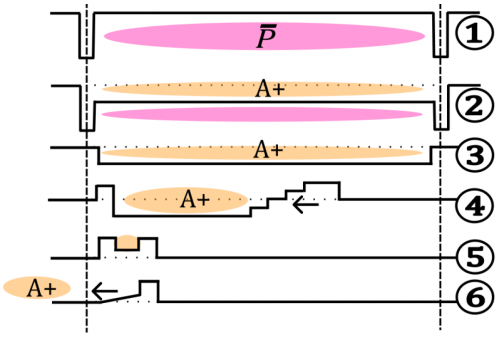

Figure 1: Ion capture process using Penning-Malmberg trap

To briefly summarize the ion capture process inside the trap (as visualized in Figure 1):

1 - Trap antiprotons in between two walls. This is made by creating two narrow potential wells that traps positive ions. Between those wells, negatively charged ions can be trapped because the well potential is lower than the ground.

2 - Lower floor potential to accommodate positive ions. By lowering the potential within the two potential wells, now the nested trap can confine both positive ions (nuclear fragments) and negative ions(antiprotons) as the positive ions, previously trapped in the two potential walls at the edge, can now spill over towards the central trap.

3 - Remove the walls. After removing the walls, antiprotons will be released and only a wide potential well that traps positive ions.

4/5 - Squeeze the trap. The long trap is reduced to only one electrode in order to to confine the particles to a localized region before release.

6 - Release ions. Now the ions are released, and the time elapsed until they reach the MCP will be used to determine the mass-to-charge ratio.

2 Antiprotonic atoms

When antiprotons are injected into gaseous atoms, these atoms can capture the antiprotons to replace their electrons. Although they have the same charge as electrons, antiprotons are nearly 2000 times heavier. Due to this mass difference, antiprotons in antiprotonic atoms exist very close to the nucleus, forming deeply bound states. Antiprotons approaching the nucleus result in annihilations, releasing substantial amounts of energy. Here, we have two different modes of emitting particles: the relaxation process and the annihilation process. The relaxation process of antiprotons leads to the emission of electrons through Auger emission, resulting in the formation of a fully or nearly fully stripped nucleus. The annihilation of antiprotons and the nucleus breaks the nucleus apart into highly charged nuclear fragments, and releases mesons such as pions in the process.

This formation process of nuclear fragments can be used for nuclear structure studies as a sensitive probe in QED/QCD experiments. The antiproton experiences a powerful electromagnetic field due to the proximity of its orbit to the nucleus. If we can accurately probe these orbits of antiprotonic atoms inside the trap, we can test strong field QED. Once the antiproton approaches the nucleus, then its orbits will be perturbed by the strong nuclear force. The study of these orbits close to the nucleus allows us to benchmark QCD. Also, by studying the resulting fragments of these annihilations, we can reveal information about the internal structures of the nucleus, such as the distribution of protons and neutrons at the surface of the nucleus, such as the neutron skin.

3 TOF (time-of-flight) spectrum analysis

3.1 Calculating mass-to-charge ratio

In the November 2023 run, antiprotons were injected into ultra-low pressure ($< 10^{-8}$mbar) Nitrogen gas, producing time-of-flight (TOF) spectrum and scintillator signals. The TOF spectrum comes from the ions created after the interaction with antiprotons, either from direct collisional ionization or Auger ejection of electrons after its capture, flying towards the MCP, while scintillator signal comes from the annihilation process.

Given the information of the electric field, we then can calculate the mass-to-charge ratio of ions producing signals using the TOF spectrum. This uses two equations defining the energy of the ions - the kinetic energy $E_k = \frac{1}{2}mv^2$ and energy from the applied potential $E = qV$. Using these equations, we get the equation for mass-to-charge ratio.

$$\frac{m}{q} = \frac{2V}{v^2} = 2V\frac{t^2}{d^2} \tag{1}$$

One issue when using this equation is that we cannot use the voltage value as how we have set that on the electrode. In fact, we end up having a parabolic potential, as the potential we applied is at the ring electrode at the shell of the cylinder. Field simulation gives the result that the field at the center of the cylinder should be around 90% of the applied voltage, and numerical approach assuming the cylindrical potential

$$\frac{1}{r}\frac{\partial}{\partial r}\left(r\frac{\partial V}{\partial r}\right) + \frac{\partial^2 V}{\partial z^2} = 0 \tag{2}$$

can be done using the Bessel function

$$R(r) = AJ_0(\sqrt{\lambda}r) + BY_0(\sqrt{\lambda}r) \tag{3}$$

that yields $V = 0.942V_0$ where V_0 is the applied voltage.

However, neither of these does not provide exact potential experienced by the ions, and can always change by the alterations in trap settings. Thus, we define a new term **Mass-to-charge constant** C_{mq} that no more requires distance and potential to be calculated explicitly:

$$\frac{m}{q} = 2V\frac{t^2}{d^2} = (C_{mq})^2 t^2 \tag{4}$$

$$(C_{mq} = \sqrt{2V}\frac{1}{d}) \tag{5}$$

$$[C_{mq}] = \frac{\sqrt{kg}}{s^{\frac{3}{2}}\sqrt{A}} \tag{6}$$

that now changes the relation between the mass-to-charge ratio and time elapsed for the particle to arrive at MCP with a constant, that should be kept the same for the same setup.

Note that the equations 4 and 5, at this stage, are only the simplest approximation and do not contain other physics that affect the motion of charges, such as acceleration inside the trap.

3.2 TOF signal analysis

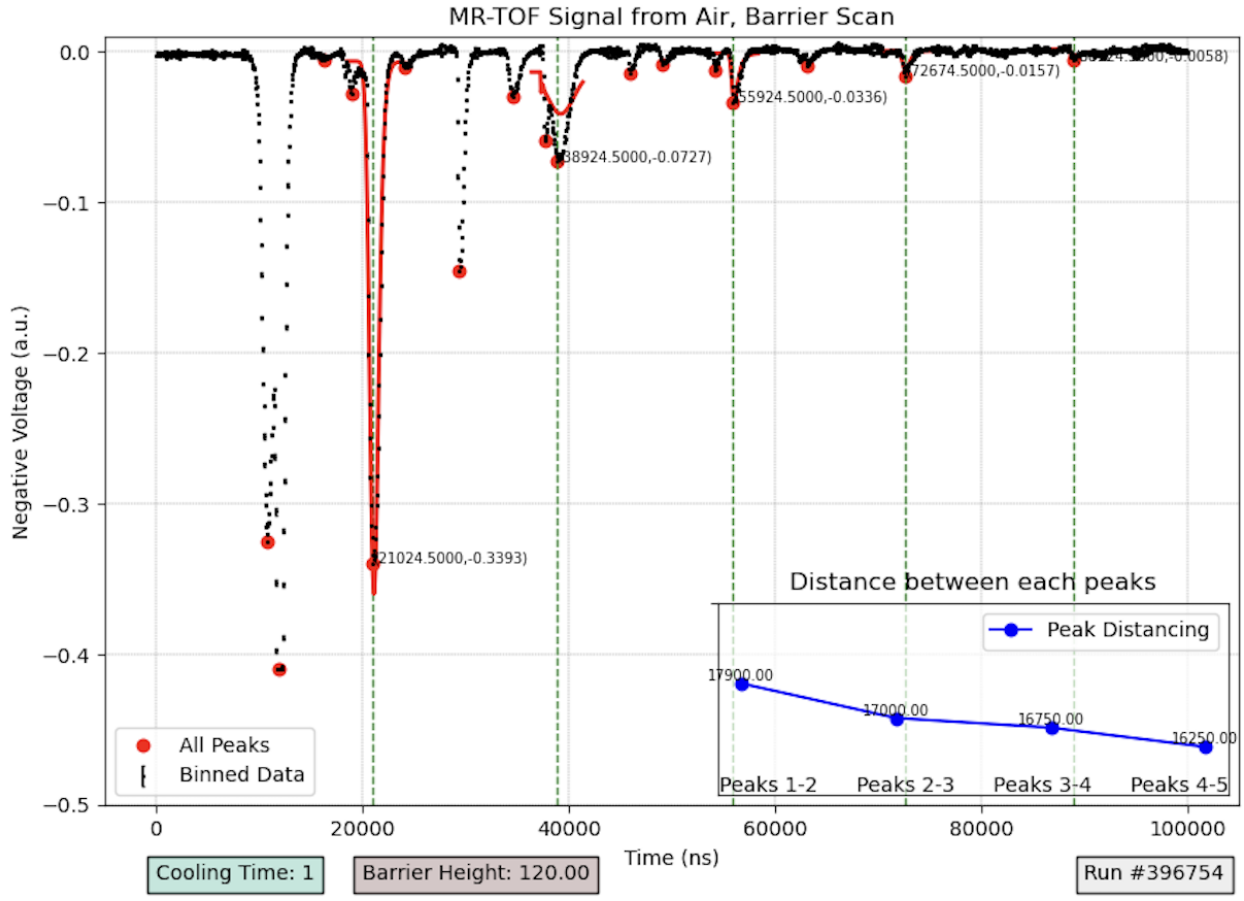

(a) TOF signal scan result from Run 396754

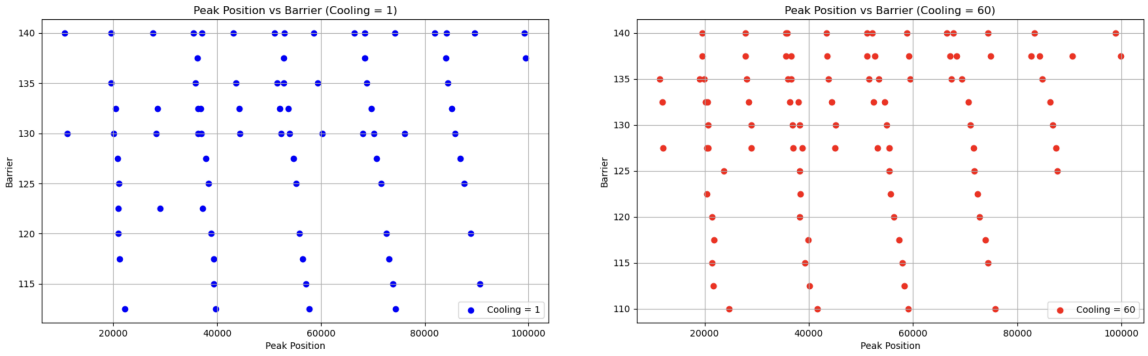

(b) Consolidated results with various barrier heights, sorted by ion storage time (Left: 1s storage, Right: 60s storage)

Figure 2: Barrier scan TOF signal analysis

Figure 2 presents a sample analysis result. During the technical development of this measurement technique, ions were released towards the MCP, but with a biased electrode as a barrier located at 0.5m downstream. This acts as an energy filter for the ions. As a

result, a resonating signal is created, caused by the bouncing of ions inside the trap with ion spilling over the barrier, which could be detected as a repeating pattern in Figure 2a. In this measurement, multiple runs were conducted with the height of this barrier (voltage applied to the barrier electrode) getting lowered after each run to see the change in peak positions with different barrier heights, where the ions were released by rapidly lowering the wall.

One thing to note is that the peak size (amplitude) and the distance between peaks (blue inset plot in Figure 2a) change as it progresses. The size of the peak and the distancing between the peaks decreases as the time progresses. The change in peak size is mostly because of the bouncing nature. Initially, the ions in the release bunch have a certain thermal distribution. After the first bounce, ions that cannot surpass the energy barrier will continue to travel between the MCP and the barrier. After thermal redistribution among these ions, at the next encounter of the barrier, fewer ions will remain in between. As a result, fewer ions will hit the MCP per each bounce, thus the peak size diminishes.

The primary cause of the decrease in peak distancing suggests that the ions are accelerated in the due course. The cause of this is still under investigation, while one possible explanation is that the radial energy is transferred to axial energy through the buffer gas cooling.

In Figure 2b, the peak locations of runs with various barrier heights are presented per respective ion storage time. For each horizontal line (peak locations for given barrier height) we can see the decreasing of ion speed due to heat loss. A vertical linear trend can be extracted from the peak locations, which is the change of peak location by changing the barrier height. Here, it is shown that when the barrier is lowered, each bounce takes longer (the distance between peaks is increased). This is because having a lower barrier results in the lower mean energy of those ions that did not pass the barrier when bouncing.

The barrier scan results can be classified into two ion storage times - 1s storage and 60s storage. In the results shown in Figure 2b, the peak positions can be grouped in a series of vertical sloped lines, which shows the rate of change of peak position by barrier height. Then, a steeper (negative) slope would suggest that the rate of change of peak position is lower in that case. It was shown that by comparing slopes in the two storage times, 60s storage showed higher rate of change of peak position by barrier height.

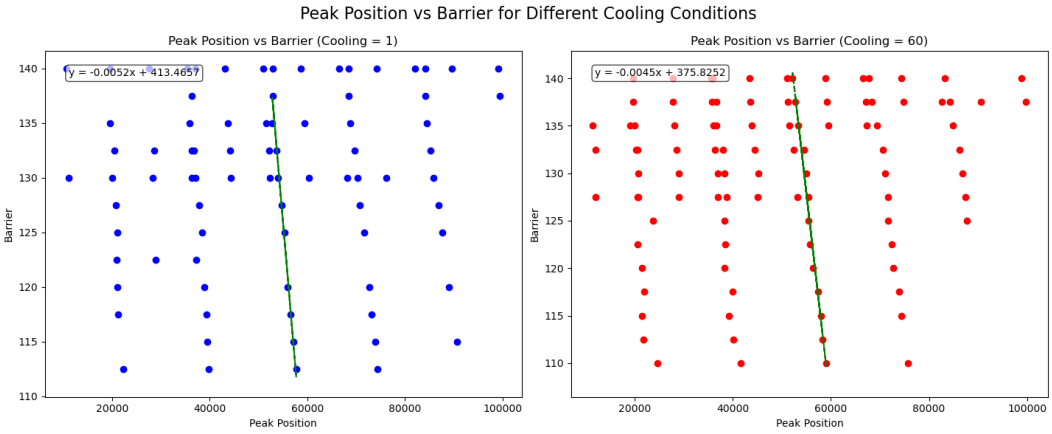

Figure 3: Comparing slope (rate of change of peak by barrier height) of each stroage time

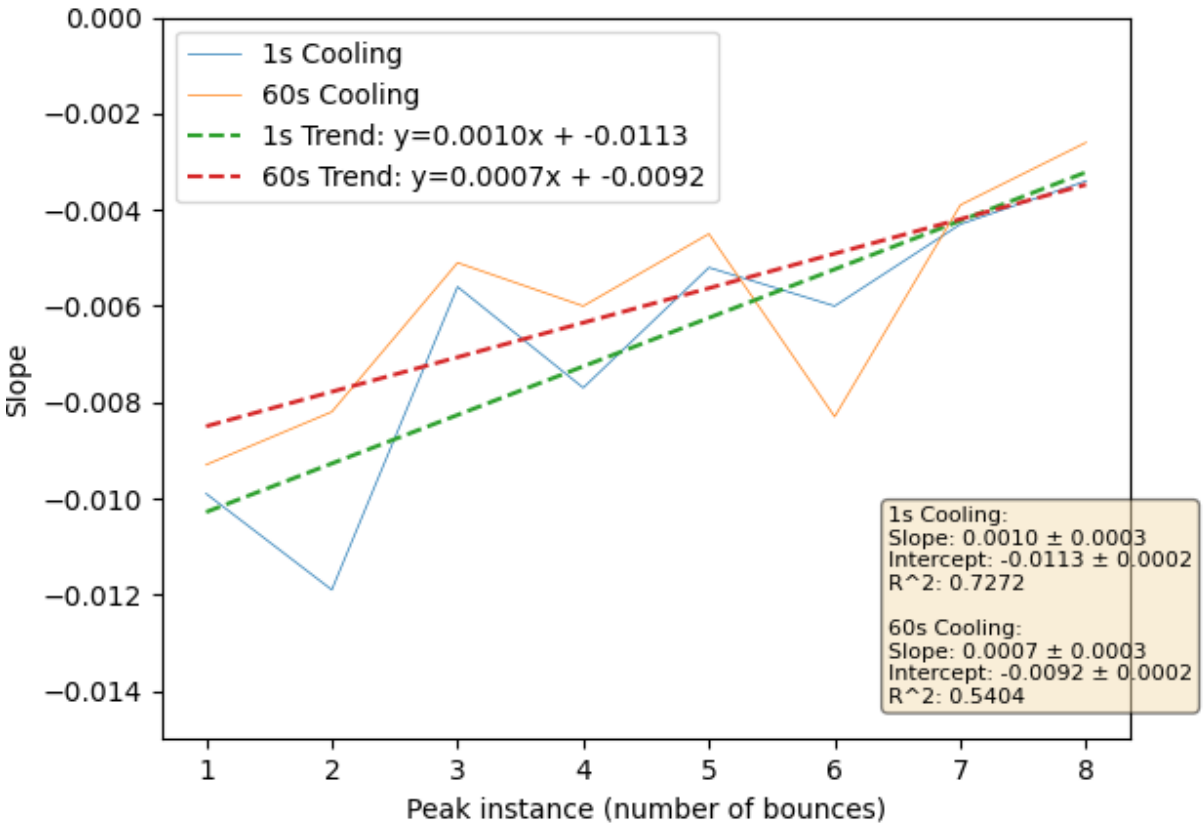

Figure 4: Comparing how the peak position changes by ion storage time.

The result in Figure 4 is obtained by the slope calculated in data like Figure 3. The peak position data obtained in the barrier scan runs are displayed as in Figure 2b, then peaks could be sorted into multiple vertical "groups". The slope of the line that connects the peaks in each group means the rate of change of peak position (timing when the bouncing occurred) due to barrier height. Then, the slopes are collected to make the plot in Figure 4. The steeper slope in the 1s storage time can then suggest that in this case the peak position changes less rapidly when the barrier height is lowered.

One hypothesis of peaks being more dispersed when the barrier is lowered is the amount of ions lost after each bounce. When the ions encounter the barrier, with lower barrier height, it is expected that more ions are lost as a larger portion of the thermal distribution within the ions will surpass the lower energy barrier. Thus, after each bounce, the mean thermal energy will drop faster in the lower energy barrier case, resulting in the faster decrease of velocity, which is the peaks getting further away from each other.

In the same manner, from the result showing that the 60s storage time showed a higher rate of change of peak position by barrier height, it can be concluded that a longer storage time leads to more energy loss (cooling), which is a cause of having a less steep slope. However, it still should be further clarified whether the cooling happens, and further studies are required to confirm this hypothesis.

3.3 Argon campaign

Now that we have the mathematical methods for the time-of-flight analysis and qualitative method to analyze signals, we can proceed to the analysis of experiment data. In this year's experiment, a pulse of antiproton beam was injected to the vacuum chamber filled with low pressure ($< 10^{-7}$mbar) Argon gas.

In this campaign, the main goal is to investigate the underlying mechanism of the stripping and fragmenting process that requires such high energy. To understand better the formation mechanism, this year's experiment was conducted using a noble gas - Argon. Forming HCI fragments from noble gases is expected to require larger energy compared to Nitrogen, thus if fully stripped fragments are observed, then we can exclude the direct collisional ionization from the formation process.

4 Analysis Results

This section presents and explains the analysis results of this year's Argon run.

4.1 Obtain, visualize, and categorize data

In the AEgIS environment, all run data is processed and stored in a central server. Clients can access and analyze data using the ALPACA package (All Python Analyses Code of AEgIS). It obtains data from the DAQ and process it through multiple pipelines (Bronze/Silver/Gold) to calculate observables that can be used for analysis.

Each run data consists of TOF signal (Captorius), scintillator signals to detect annihilation, images obtained from MCP, and various configuration details for that run. Using the TOF signal, the plot like what is presented in Figure 5 can be drawn. In case the noise level hampers the clarity of visualization, additional measures like binning or low-pass filter can be applied.

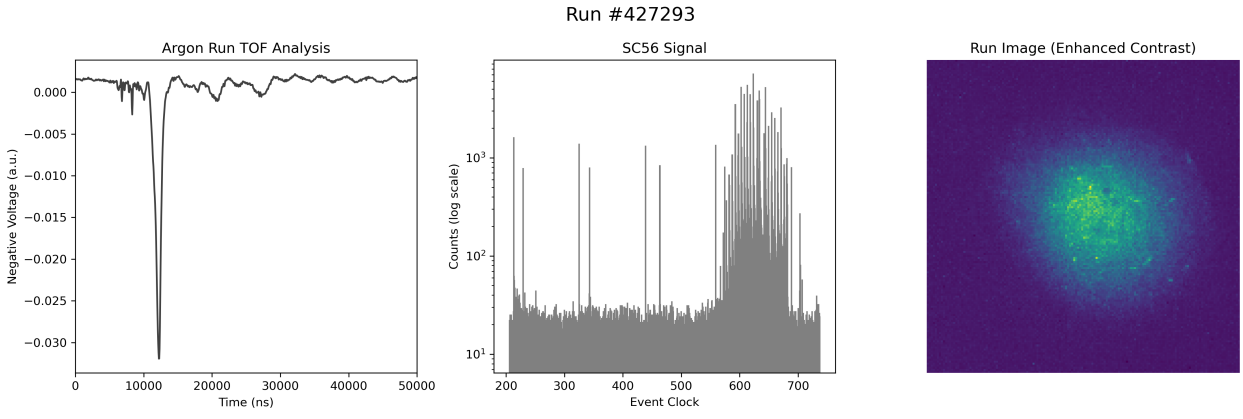

Figure 5: Sample data from Argon run. From left to right, TOF signal from MCP, scintillator signal, and the image from MCP is shown.

In Figure 5, the plot presented on the left, which is the TOF signal, has been processed using both binning and low-pass filter. For this dataset, a Butterworth filter was applied to smooth the signal by removing the high-frequency noise components. A *flitflit* function was used to ensure that the filtering does not distort the phase of the original signal. Plot in the middle is the signal from the scintillator, where the peaks in the signal indicates annihilation signals. On the right is the image obtained from MCP, which visualizes the incident signals to the detector.

During the whole campaign, as data from multiple runs are being accumulated, it is crucial to keep track of each runs in terms of how they were made. To distinguish runs with desired conditions (scripts, observable, timestamp, and whether they have the right amount of data to produce plots), an external HTML document was written to help filtering and exporting desired dataset.

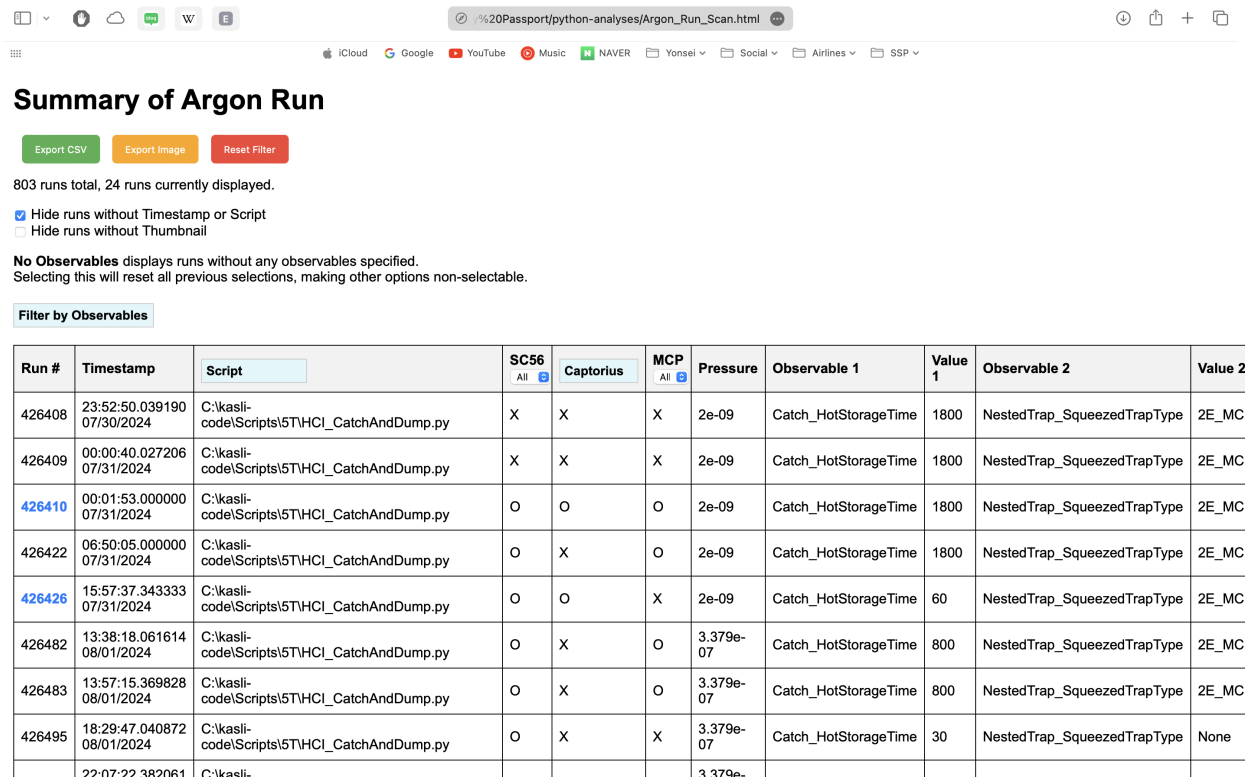

Run #	Timestamp	Script	SC56 All	Captorius	MCP All	Pressure	Observable 1	Value 1	Observable 2	Value 2
426408	23:52:50.039190 07/30/2024	C:\kasli-code\Scripts\5T\HCI_CatchAndDump.py	X	X	X	2e-09	Catch_HotStorageTime	1800	NestedTrap_SqueezedTrapType	2E_MC
426409	00:00:40.027206 07/31/2024	C:\kasli-code\Scripts\5T\HCI_CatchAndDump.py	X	X	X	2e-09	Catch_HotStorageTime	1800	NestedTrap_SqueezedTrapType	2E_MC
426410	00:01:53.000000 07/31/2024	C:\kasli-code\Scripts\5T\HCI_CatchAndDump.py	O	O	O	2e-09	Catch_HotStorageTime	1800	NestedTrap_SqueezedTrapType	2E_MC
426422	06:50:05.000000 07/31/2024	C:\kasli-code\Scripts\5T\HCI_CatchAndDump.py	O	X	O	2e-09	Catch_HotStorageTime	1800	NestedTrap_SqueezedTrapType	2E_MC
426426	15:57:37.343333 07/31/2024	C:\kasli-code\Scripts\5T\HCI_CatchAndDump.py	O	O	X	2e-09	Catch_HotStorageTime	60	NestedTrap_SqueezedTrapType	2E_MC
426482	13:38:18.061614 08/01/2024	C:\kasli-code\Scripts\5T\HCI_CatchAndDump.py	O	X	O	3.379e-07	Catch_HotStorageTime	800	NestedTrap_SqueezedTrapType	2E_MC
426483	13:57:15.369828 08/01/2024	C:\kasli-code\Scripts\5T\HCI_CatchAndDump.py	O	X	O	3.379e-07	Catch_HotStorageTime	800	NestedTrap_SqueezedTrapType	2E_MC
426495	18:29:47.040872 08/01/2024	C:\kasli-code\Scripts\5T\HCI_CatchAndDump.py	O	X	X	3.379e-07	Catch_HotStorageTime	30	NestedTrap_SqueezedTrapType	None

Figure 6: A HTML-based run information database, capable of filtering and exporting dataset

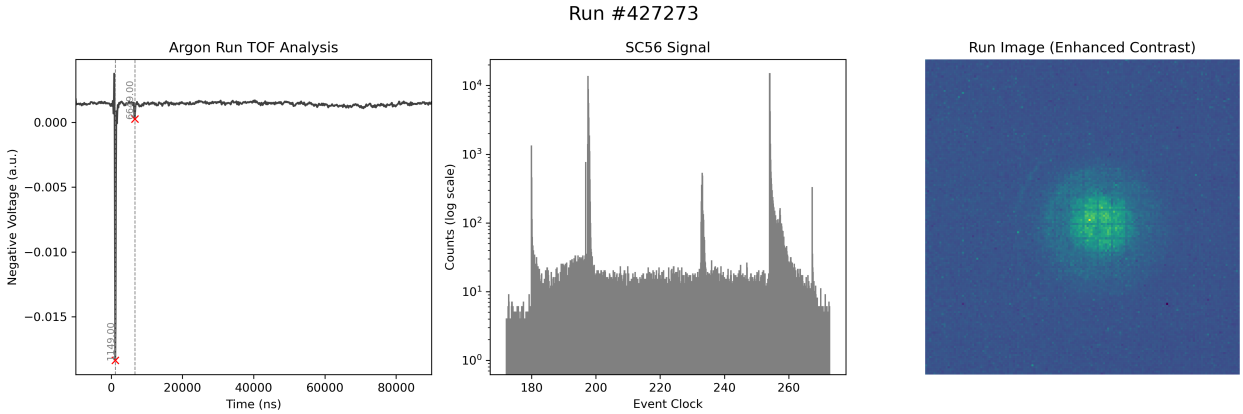

Figure 7: Plot of antiproton calibration run

4.2 Antiproton calibration and mass-to-charge constant

Before moving onto the result analysis, a calibration run should be conducted to provide a reference point for determining how to connect the peak position in TOF signal and the corresponding mass-to-charge ratio. In the calibration run, negatively charged particles, electrons, and antiprotons are inhabited in the same trap used for positively charged ions, but with the opposite potential to house the negative ions. The release of electrons and antiprotons in this setup can be used as reference as the mass-to-charge ratio of these species are already known. This is used to calculate a new constant called the mass-to-charge constant, which is fixed given that the setup is maintained.

Although the detailed setup information of each run is contained in the run data, as explained above, it is hard, and often not accurate to calculate applied potential and travel distance separately and explicitly. Here, mass-to-charge constant could be a good initial approximation, although it still contains deviations from real data, mainly caused by the non-constant acceleration of charges inside the trap.

As now the data is organized, the calibration run results can be examined to provide the mass-to-charge constant value for further analysis. In the calibration runs, trap potentials were flipped so that only the negative ions are captured and released. In this case, contained ions cannot be ejected to the MCP. These runs are indicated by the script used to initiate(HCI_pbar_calibration.py), which could be filtered using the HTML database presented above (Figure 6).

Figure 7 shows the plot of an antiproton calibration run. The second peak, which is now located at 6649ns, will be considered as a reference point for antiprotons, which has a mass-to-charge ratio of 1. Recalling the equation for mass-to-charge constant,

$$\frac{m}{q} = 2V\frac{t^2}{d^2} = (C_{mq})^2 t^2 \tag{7}$$

$$C_{mq} = \sqrt{\frac{m}{q}}\frac{1}{t} \tag{8}$$

this gives us the mass-to-charge constant of $C_{mq} = \frac{1}{6.649*10^{-6}} = 1.504 * 10^5$. This value can

be used for analyzing other runs with Argon gas inside the same trap.

Justification of selecting the second, smaller signal rather than the larger, leftmost one can be provided by calculating the travel distance using mass-to-charge constant. This calibration run is conducted with the floor potential of V = 150V, and from the actual geometry of the trap, the travel distance corresponds to 1m.

In Figure 7, the first large peak appears at t = 1149ns. As this is appearing before the second peak, it could be assumed that this corresponds to another particle inside the trap - electrons. Electrons are known to have a mass-to-charge ratio of $5.686 * 10^{-12} \frac{kg}{C}$. Using V = 150V and plugging into Equation 7, we get $d = 8.35m$, which is far off from the real geometry, even considering that it should not be exactly 1m due to potential field as explained in section 3.1. When calculating the travel distance using the second peak as above, using m/q = 1 for antiproton and t = 6649ns gives $d = 1.131m$, which is a much better approximation.

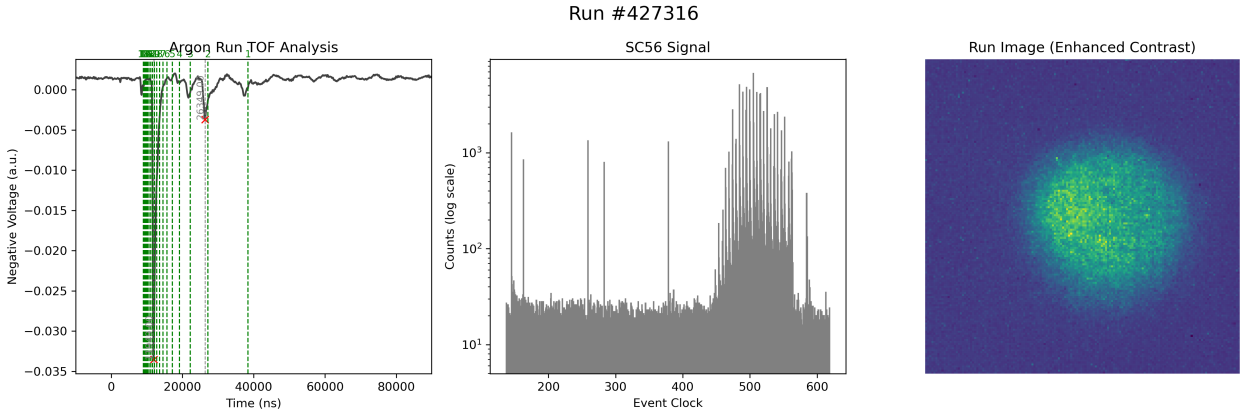

(a) Complete run analysis of an Argon run

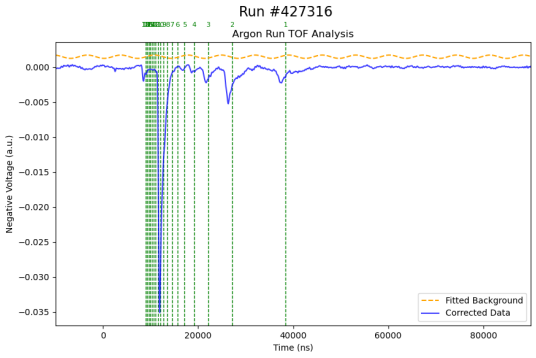

(b) TOF signal with reduced background

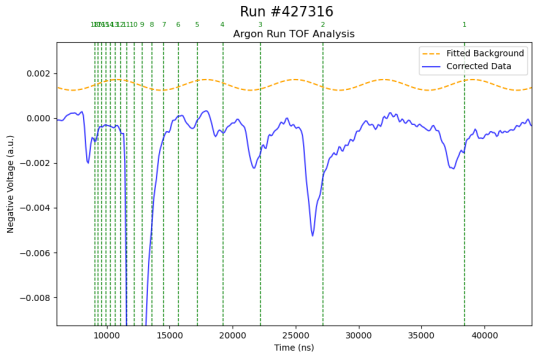

(c) Mass-to-charge of peaks

Figure 8: Overall analysis result of sample Argon run.
(Note: For 8b, as a result of removing background signal that comes after the large peak, a new sinusoidal background has been introduced to the signal before that.)

4.3 Sample Argon run result

Using the previously calculated mass-to-charge constant, we now have the relation between the mass-to-charge ratio and the peak position:

$$\frac{m}{q} = (1.504 * 10^5)^2 * t^2 \tag{9}$$

In case where the trap potential changes, it should be:

$$\frac{m}{q} = (1.504 * 10^5)^2 * \frac{V}{150} * t^2 \tag{10}$$

as the calibration run used 150V trap floor potential.

When analyzing run results, some additional measures can be taken to aid the process. Figure 8a is one example of the analysis result of the Argon run. Here, each points that refers to the ion state of Argon is marked. Each point corresponds to the point where the mass-to-charge ratio is $\frac{40}{18}$, $\frac{40}{17}$, $\frac{40}{16}$, $\frac{40}{15}$, $\frac{40}{14}$, ..., $\frac{40}{1}$, which corresponds to the ion state of the most prevalent Argon isotope (^{40}Ar): $^{40}Ar^{18+}$, $^{40}Ar^{17+}$, $^{40}Ar^{16+}$, $^{40}Ar^{15+}$, $^{40}Ar^{14+}$, ..., $^{40}Ar^{1+}$.

Another consideration was the background noise. A sinusoidal background was removed to make peaks more clearly visible. This background is likely to come from the capacitor behavior of RC circuit inside the MCP, after receiving a large signal. In Figure 8a, the TOF signal was not treated with any background reduction. Compared to that, Figures 8b and 8c were drawn with consideration of the sinusoidal background. As a result, the background signal has been flattened (at the regions after the largest signal peak) and is now centered around zero.

One way to validate this result is to calculate the mass-to-charge constant of this result. Using the peak position that was acquired in the experiment, Equation 8 provides "experimental mass-to-charge constant". Here, it will be compared to the previously obtained value from the antiproton calibration: $C_{mq} = 1.504 * 10^5$.

Charge state	$^{40}Ar^{1+}$	$^{40}Ar^{2+}$	$^{40}Ar^{3+}$	$^{40}Ar^{4+}$	$\cdots$
Position by calculation	38387.65	27144.17	22163.12	19193.83	$\cdots$
m/q	$\frac{40}{1}$	$\frac{40}{2}$	$\frac{40}{3}$	$\frac{40}{4}$	$\cdots$
Peak position	37349	26349	21649	18649	$\cdots$
Error (%)	2.97	2.93	2.32	2.84	$\cdots$
Mass-to-charge constant (C_{mq})	$1.697 * 10^5$	$1.697 * 10^5$	$1.686 * 10^5$	$1.695 * 10^5$	$\cdots$
C_{mq} Error (%)	12.89	12.85	12.15	12.74	$\cdots$

Table 1: Discrepancy between theoretical and experimental mass-to-charge constant

4.4 Peak analysis

Among multiple runs that used the same settings, there were several things in common worth noting, especially the distinctive "groups" of peaks. Among the peaks observed in each run, there are patterns in how those peaks exist in terms of position and size.

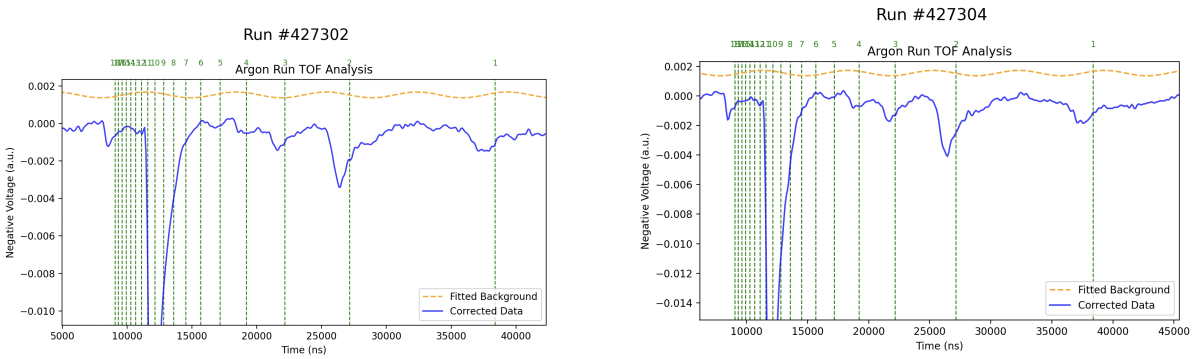

Figure 9: Other results for Argon run

First, on the leftmost region, there is one peak that appears in every run result which is further left from the $^{40}Ar^{18+}$ assumption line. This is located where the mass-to-charge ratio is around 2.2. Simulation results from previous studies suggest this could be a candidate for fully stripped fragments. Simulation data indicates that the mass-to-charge ratio of fully-stripped ions should have a distribution that peaks around m/q $\approx$ 2.2.

Figure 10: Run data with EMG (exponentially modified Gaussian) fitting

Charge state	$^{40}Ar^{1+}$	$^{40}Ar^{2+}$	$^{40}Ar^{3+}$	$^{40}Ar^{4+}$	···
Peak position	37349	26349	21649	18649	···
Fit centroid	37050	25953	21299	18407	···
Fitting uncertainty (ns)	28.76	10.69	13.41	11.80	···

Table 2: Fitting uncertainties

Next, the peaks on the right-hand side. These peaks, which are shifted to the left from the peak approximation using calculated m/q values, deviate from the calculation for around 3%. (See "Error" values from Table 1.) It is worth noting that this error rate could not be explained by the uncertainty in finding and fitting peaks. (See Figure 10) This uncertainty refers to the uncertainty in the estimated centroid, so that smaller error value indicates a more precise estimation of centroid, meaning that the fitting is well-defined. However, these uncertainty values are a very preliminary estimation, since the use of certain fitting function (exponentially modified Gaussian) should be validated.

In all cases, the size of the peak at Ar^{2+} is the largest, decreasing on either side. It is known that the direct collisional ionization of antiprotons cannot provide sufficient energy to remove more than a few electrons. Thus, the relative abundance of the higher Argon charge states compared to Ar^{1+} should be interpreted by introducing other origins of forming ions. High velocity fragments could also ionize the Argon gas. Inside the trap, by annihilation at the nucleus of an antiprotonic atom, HCIs are formed, which have high energy due to the nature of the annihilation process. This can provide more energy to the Argon atom than the original antiprotons, thus are capable of producing higher charge states.

Finally, there is one largest peak, located around the mass-to-charge ratio of 4. As this peak dominates all other signals in every run, it is rather challenging to conclude this as Ar^{10+}. One of the possibilities of having such a uniform and strong signal is the Helium ion, specifically, $^{4}He^{1+}$. However, this hypothesis should be further validated. It has to be ensured that there are indeed Helium ions in the trap and that the ionization energy provided either from antiprotons or HCIs is sufficient.

5 Conclusion

In this report, the analysis procedure and results of synthesizing highly charged radioactive ions (HCIs) in a Penning-Malmberg trap using Argon have been explained. By pulsing antiprotons into a nested trap with low-pressure gas, it was revealed that ions with various charged states were formed. One of the possible causes of the formation of high charge-state ions of noble gas like Argon could be a result of HCI from antiproton annihilations, and the result showed a signal at the location where fully-stripped ion fragments are expected to exist. However, further studies are needed to confirm the origin of the peak.

Using the method analysis used in this report, it was shown that time-of-flight (TOF) mass spectrometry could provide signal data of the capturing of HCIs and ions. Calculating the mass-to-charge ratio based on its arrival time at the MCP could provide information about peaks appearing at the TOF spectrum and which charge state it should correspond to.

There are still some points to be improved, or to be further studied. More clear explanations of the cause of deviations in between peak positions in TOF signal by calculation and experiment. The largest signal in every signal should also be explained. Being located at the mass-to-charge of 4, it could be either $^{4}He^{1+}$, or other ion fragments. One possible way to verify this is to examine the substructures. The substructures can formed by a sum of signals caused by nuclear fragments, and by He^{1+}/He^{2+} ion contamination which are formed. This can be achieved by implementing measurements with higher resolution.